International Journal of Heat and Mass Transfer 52 (2009) 1365–1373

Contents lists available at ScienceDirect

International Journal of Heat and Mass Transfer

journal homepage: www.elsevier.com/locate/ijhmt

Distributed dynamic modeling and experimental study of PV evaporator in a PV/T solar-assisted heat pump

Jie Ji [a,*], Hanfeng He [a], Tintai Chow [b], Gang Pei [a], Wei He [a], Keliang Liu [a]

[a] Department of Thermal Science and Energy Engineering, University of Science and Technology of China, 96 Jinzhai Road, Hefei, Anhui, People's Republic of China
[b] Division of Building Science & Technology, City University of Hong Kong, Tat Chee Avenue, Kowloon, Hong Kong SAR, People's Republic of China

ARTICLE INFO

Article history:
Received 23 November 2007
Received in revised form 14 July 2008
Available online 20 October 2008

Keywords:
PV direct-expansion evaporator
Photovoltaic/thermal
Solar-assisted heat pump

ABSTRACT

A novel photovoltaic/thermal solar-assisted heat pump (PV/T-SAHP) system is described in this paper. A specially designed direct-expansion evaporator (PV evaporator), which is laminated with PV cells on the front surface of the thermal absorber, has been adopted in our system to acquire simultaneously thermal energy and electricity from solar radiation. A dynamic model of the PV evaporator based on the distributed parameter approach is also presented. Given the instantaneous solar irradiance and ambient temperature, the numerical model is able to output the spatial distributions of refrigerant conditions, including pressure, temperature, vapor quality and enthalpy. A two-dimensional temperature distribution of the evaporator body is also computed. Comparisons between the simulation results and the experimental measurements show that the model is able to give satisfactory predictions. The results show that high electrical and thermal performance can be achieved. The PV efficiency and thermal efficiency are above 12% and 50% during the testing period.

1. Introduction

Solar energy, well known as a clean and inexhaustible energy source, has received much attention in the past decades. Among the diversifying research endeavors, photovoltaic and solar-assisted heat pump are two promising yet very different technologies. A photovoltaic (PV) system consists of interconnected solar cells which convert photons directly into electron flow. A direct-expansion solar-assisted heat pump system (DXSAHP) directly integrates Rankine refrigeration device with solar thermal collector. The solar collector serves as an evaporator where the refrigerant absorbs thermal energy from solar radiation.

The concept of DXSAHP was firstly presented by Sporn and Ambrose in 1955 [1]. Since 1970s it has undergone substantial developments, as a response to the global concerns like the energy crisis and the global warming issues. Compared to the air-source heat pump system, the DXSAHP operates at higher evaporating temperature and therefore with higher heat pump COP (coefficient of Performance). Numerous theoretical and experimental studies have been done by researchers worldwide. To name some examples, Chaturvedi et al. [2] investigated the thermal performance of a variable capacity DXSAHP in which bare solar collector and variable frequency compressor were employed. Torres-Reyes et al. [3,4] studied a DXSAHP both theoretically and experimentally; thermodynamic optimization was performed. Kuang and Wang [5] investigated the long-term performance of a multi-functional DXSAHP designed for domestic use, through which space heating was offered in winter, air conditioning in summer, and hot water throughout the year round; the DXSAHP was shown able to support long-term operation under a wide range of weather conditions at low running cost. Huang et al. [6,7] presented an integral-type solar-assisted heat pump (ISAHP) which was able to absorb heat from solar radiation and ambient air simultaneously; computer simulations were executed to analyze the daily system performance.

For PV technology on the other hand, it is a well-known fact that the electricity generating efficiency of solar cells drops with the increase in operating temperature. A photovoltaic/thermal (PV/T) system, which applies a coolant onto the solar cells, can override such a limitation by bringing down its operating temperature and re-utilizing the captured heat energy. Since 1970s, many researchers have performed theoretical and/or experimental investigations on PV/T systems. Their efforts were focused on using either air or water as the coolant. Again to quote some examples, as early as in 1979 Kern and Russell [8] used the simulation tool TRNSYS to investigate a water-type PV/T collector which supplied thermal energy to a heat pump. Huang et al. [9] introduced the concept of primary-energy saving efficiency for the evaluation of water-type PV/T systems. More recently, our collaborative efforts in China developed a new water-type PV/T collector that adopts a flat-box thermal absorber design [10–12]. Performance analyses

* Corresponding author. Tel./fax: +86 551 3601652.
E-mail address: jijie@ustc.edu.cn (J. Ji).

0017-9310/$ - see front matter © 2008 Elsevier Ltd. All rights reserved.
doi:10.1016/j.ijheatmasstransfer.2008.08.017

Nomenclature

A	surface area, m^2
C	specific heat of solid, J/(kg K)
D	pipe diameter, m
E	output electricity, W
f	friction factor, –
G	solar irradiance, W/m^2
h	specific enthalpy, J/kg
l	effective thickness, m
m	mass, kg
$\dot{m}$	mass flow rate, kg/s
P	refrigerant pressure, Pa
Q	thermal heat gain, W
$\dot{q}$	heat flux, W/m^2
R	thermal resistance, K/W
r	reflectivity, –
T	temperature, K
t	time, s
u	flow velocity, m/s
x	vapor quality, –

Subscripts

a	air; ambient
b	back
c	thermal collector
d	dry-out
f	friction
G	gas
in	internal
L, l	liquid
p	pipe
pv	photovoltaic
r	refrigerant; radiation
ref	reference conditions
t	thermal
tp	two-phase
v	vapor

Greek letters

α	heat transfer coefficient, $W/(m^2\,K)$
β	absorptivity, –
ε	emissivity, –
η	efficiency, –
θ	angle, degree
λ	thermal conductivity, W/(m K)
μ	dynamic viscosity, Pa s
ξ	PV cell coverage ratio, –
ρ	average density, kg/m^3
σ	Stefan–Boltzman constant, $W/(m^2\,K^4)$
τ	transmissivity of EVA, –
$(\tau\beta)$	effective absorptivity, –

through dynamic simulation and experimental work were conducted. Tripanagnostopoulos et al. [13] presented two modified air-type PV/T systems. A theoretical model was also developed to study the effects of the channel configuration and air flow rate on the electrical and thermal characteristics.

These previous studies have indicated that using water as the coolant is more effective than using air due to the more favourable thermo-physical properties [14]. Nevertheless, for supporting practical heating applications, the hot water temperature has to reach at least 40 °C. This temperature requirement unavoidably lowers down the cooling effect of the PV system. To achieve better cooling effect, refrigerant in an evaporator can be alternatively used because of its relatively low and steady working temperature. A specially designed PV/T collector, which can be used as the evaporator of a DXSAHP, is presented in this paper. This PV evaporator combines the two above mentioned solar technologies in a single system for the dual production of electricity and heat energy. While a fraction of the solar energy incident on the PV evaporator is converted to electricity by the PV cells, most of the remaining portion is converted to heat energy which is absorbed by the refrigerant. The direct expansion of refrigerant inside the copper coil transfers the absorbed heat energy to the condenser. At the same time, the PV cells are able to operate at some low and stable temperature conditions. This improves the electrical yield of the system.

2. Structure of PV evaporator module

The structure of our PV evaporator module is shown in Fig. 1. A single PV evaporator module including the aluminum alloy frame is of dimensions 1.01 m × 0.73 m. The functional part of the evaporator module is a hybrid solar collector with solar cell encapsulation laminated on to the front surface of a thermal absorber panel. The solar cells are packed between two transparent TPT (tedlar-polyester-tedlar) layers, with EVA (ethylene-vinyl acetate) acting as a uniform intermediate layer to conglutinate them. The basic panel of the collector is composed of a 1.5 mm thick aluminum alloy plate and a 0.5 mm thick aluminum plate. A copper coil 6.0 m long with 7 mm outer diameter and 6 mm inner diameter is positioned in six U-type grooves which are formed by the two aluminum plates. The spacing (W) between two adjacent grooves is 130 mm. In order to improve the thermal performance of the evaporator in cold winter, a glass cover and a thermal insulation layer are provided, respectively, at the front and the back of the module. The glass cover is designed for easy removal where necessary. The search without glass cover is discussed in this paper.

The PV evaporator array in our system consists of nine (3×3) PV evaporator modules, which are facing south at a tilt angle of 38°. Every three of them are connected in series to form a column and in turn the three columns are connected in parallel. The total irradiation (thermal collector) area is 5.49 m^2 and the total PV cell area is 4.59 m^2. Taking advantage of the symmetry, the numerical model has been developed based on one single column that carries three evaporator modules in series.

3. Mathematical model

The distributed modeling approach has been widely used to simulate the behavior of the dry-expansion evaporator in the past decades. MacArthur et al. [15] presented a dynamic model of the evaporator based on homogeneous flow; the momentum exchange between liquid and vapor in the two-phase flow region was ignored and the evaporating temperature was considered unchanged. In Wang's model [16], the momentum equation was considered as time-independent and the temperature of the refrigerant in the two-phase flow region was taken as constant. Tso et al. [17] developed a generalized distributed parameter model to analysis both the steady and transient behavior of dry-expansion evaporators; experimental work was conducted for model verification.

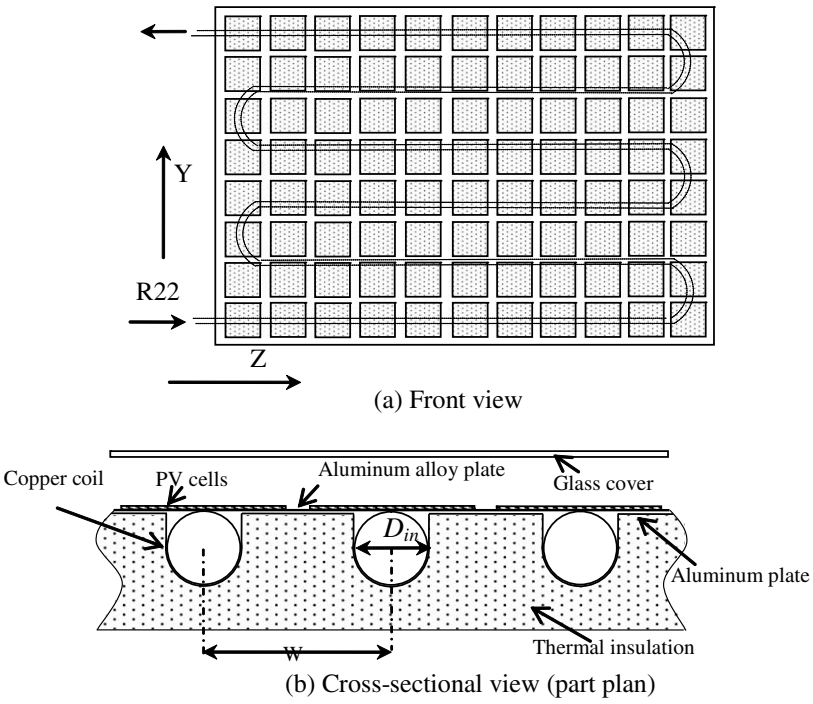

Fig. 1. Structure of a PV evaporator module.

In this paper, we introduce a dynamic distributed parameter model of the above mentioned PV evaporator. In this model, the two-phase flow inside the copper coil is taken as homogeneous. The mathematical model is composed of three main equation sets: (i) heat balance equation of the PV module, (ii) two-dimensional heat conduction equation of the thermal collector which includes the basic panel and copper coil, and (iii) conservation equations of the refrigerant flow. The influence of the pressure drop on the physical properties of the liquid and vapor refrigerant, such as temperature, density and enthalpy, has been taken into account.

3.1. Heat balance equation of the PV module

The thermal resistance at the surface of contact leads to a temperature differential between the PV cells and the aluminum plates [18]. Our experimental test detected a temperature difference ranged from 3–15 °C between the two. In our model, as shown in Fig. 2, the PV cells and the thermal collector segments are represented by separate control volumes (nodes). Uniform temperature of all PV cells is assumed. Each PV cell node is positioned at the center of the surface of the corresponding discrete control volume of the basic panel. The heat balance equation is established as:

$$l_{pv}\rho_{pv}C_{pv}\frac{\partial T_{pv}}{\partial t} = G(\tau\beta)_{pv} - E + \alpha_{a\text{-}pv}(T_a - T_{pv}) + \alpha_{r,\,a\text{-}pv}(T_{sky} - T_{pv}) + \frac{T_c - T_{pv}}{R_{pv\text{-}c}} \quad (1)$$

where l_{pv}, ρ_{pv} and C_{pv} are, respectively, the effective thickness, density and specific heat of the PV cells; R_{pv-c} is the contact thermal resistance between the PV cells and the thermal collector; α_{a-pv} and $\alpha_{r,a-pv}$ are, respectively, the convective and radiant heat transfer coefficients between the PV cells and the ambient; G is the solar irradiance; $(\tau\beta)_{pv}$ is the effective absorptivity of the PV cells; E is the output electricity from the PV cells.

According to Duffie and Beckman [19],

$$(\tau\beta)_{pv} = \frac{\tau_{eva}\beta_{pv}}{1-(1-\beta_{pv})\cdot r} \quad (2)$$

$$\alpha_{a\text{-}pv} = 2.8 + 3.0\cdot u_{wind} \quad (3)$$

and

$$\alpha_{r,\,a\text{-}pv} = \varepsilon_{pv}\sigma(T_{pv}^2 + T_{sky}^2)(T_{pv} + T_{sky}) \quad (4)$$

where u_{wind} is the wind speed; T_{sky} is the sky temperature given by

$$T_{sky} = 0.0552T_a^{1.5} \quad (5)$$

In Eq. (2), β_{pv} is the absorptivity of the PV cell; τ_{eva} and r are, respectively, the transmissivity and reflectivity of EVA, in that

$$\tau_{eva} = \frac{1-r}{1+r} \quad (6)$$

$$r = \frac{\sin^2(\theta_1-\theta_2)}{\sin^2(\theta_1+\theta_2)} + \frac{\tan^2(\theta_1-\theta_2)}{\tan^2(\theta_1+\theta_2)} \quad (7)$$

where θ_1 and θ_2 are, respectively, the incidence and refraction angles of the solar beam.

E is given by the instantaneous PV efficiency (η_{pv}), in that

$$E = G\eta_{pv} = G\tau_{eva}\eta_{ref}[1 - 0.0045(T_{pv} - 298.15)] \quad (8)$$

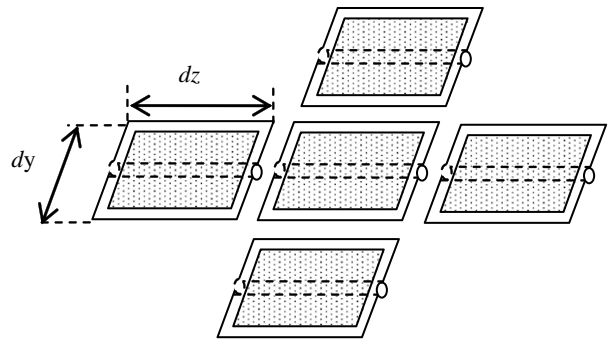

Fig. 2. Discretization of the PV/T collector plate into control volumes.

where η_{ref} is the electrical efficiency at standard conditions of 1000 W/m^2 and 25 °C.

3.2. Two-dimensional heat conduction equation of the thermal collector

The thermal collector is composed of three elements: the copper coil, the aluminum plate and the aluminum alloy plate. By neglecting the contact thermal resistance, the temperature of these three elements can be assumed as uniform at any control volume. The heat conduction equation of each control volume with lumped mass m_c, specific heat C_c, and thermal conductivity λ_c is then:

$$m_c C_c \frac{\partial T_c}{\partial t} = G(\tau\beta)_c(1-\xi)A_c + \alpha_{a\text{-}c}(1-\xi)A_c(T_a - T_c) + \alpha_{r,\,a\text{-}c}(1 - \xi)A_c(T_{sky} - T_c) + \xi A_c \frac{T_{pv} - T_c}{R_{pv-c}} + \alpha_r A_r(T_r - T_c) + A_c\frac{(T_a - T_c)}{R_b} + \lambda_{c,\,y} l_{c,\,y} A_c \frac{\partial^2 T_c}{\partial y^2} + \lambda_{c,\,z} l_{c,\,z} A_c \frac{\partial^2 T_c}{\partial z^2} \quad (9)$$

where R_b is the thermal resistance between the back of the thermal collector and the ambient; $(\tau\beta)_c$ is the effective absorptivity of the thermal collector defined in the same manner as in Eq. (2); $l_{c,y}$ and $l_{c,z}$ are the effective thicknesses along the *Y* direction and *Z direction*, respectively; and ξ is the PV cell coverage ratio defined as

$$\xi = \frac{A_{pv}}{A_c} \quad (10)$$

3.3. Conservation equations of the refrigerant

The transport process of the refrigerant taking place in the evaporator can be described mathematically by a three-dimensional coupled, non-linear partial differential equation set that governs the transport of mass, momentum and energy for a Newtonian fluid. The following assumptions have been made in our model:

(a) The refrigerant flow inside the evaporator tubing is one-dimensional and homogeneous. The liquid and vapor refrigerant have the same average transport velocity, i.e. the slip between liquid and vapor is neglected.
(b) The liquid and vapor phases are in saturated thermal equilibrium and the pressure of the liquid and vapor at the same cross-section are equal.
(c) The changes in kinetic energy and potential energy are ignored in the energy equation set.

The control volume for the refrigerant flow is shown in Fig. 3. With the above listed assumptions, a simplified dynamic flow model can be obtained as follow:

Continuity equation for the refrigerant:

$$\frac{\partial \rho}{\partial t} + \frac{\partial(\rho u)}{\partial z} = 0 \quad (11)$$

where ρ is the average density of the refrigerant and can be determined by

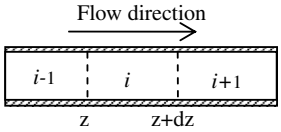

Fig. 3. Control volumes at the refrigerant tubing.

$$\rho = \frac{\rho_v \rho_l}{x\rho_l + (1-x)\rho_v} \quad (12)$$

where x is the vapor quality that carries a value of 1 in the superheated region, a value of 0 in the subcooling region, and $0 < x < 1$ in the two-phase flow region.

Momentum equation for the refrigerant:

$$\frac{\partial(\rho u)}{\partial t} + \frac{\partial(\rho u^2)}{\mathrm{d}z} = -\frac{\partial P}{\partial z} - \left(\frac{\partial p}{\partial z}\right)_f \quad (13)$$

where $\left(\frac{\partial p}{\partial z}\right)_f$ is the frictional pressure drop of the refrigerant.

Energy equation for the refrigerant:

$$\frac{\partial(\rho h)}{\partial t} + \frac{\partial(\rho u h)}{\partial z} = \frac{\pi D_{in}}{A_p}\dot{q}_r \quad (14)$$

where $\dot{q}_r$ is the heat flux at the pipe wall given by $\dot{q}_r = \alpha_r(T_c - T_r)$; h is the average specific enthalpy of the refrigerant determined by the vapor quality and the specific enthalpy at the saturated liquid and vapor states, i.e.

$$h = xh_v + (1-x)h_l \quad (15)$$

Substituting the result of Eq. (11) multiplying by u into Eq. (13) yields:

$$\rho\frac{\partial u}{\partial t} + \rho u\frac{\partial u}{\partial z} = -\frac{\partial P}{\partial z} - \left(\frac{\partial p}{\partial z}\right)_f \quad (16)$$

Eq. (14) can be modified in a similar manner, so

$$\frac{\partial h}{\partial t} + u\frac{\partial h}{\partial z} = \frac{\pi D_{in}}{\rho A_p}\dot{q}_r \quad (17)$$

3.4. Frictional loss of the refrigerant

The empirical correlation proposed by Müller-Steinhagen and Heck [20] has been employed to determine the frictional loss of the refrigerant, i.e.

$$\left(\frac{\partial p}{\partial z}\right)_f = \left\{\left(\frac{dp}{dz}\right)_{Lo} + 2\left[\left(\frac{dp}{dz}\right)_{Go} - \left(\frac{dp}{dz}\right)_{Lo}\right]x\right\}(1-x)^{\frac{1}{3}} + \left(\frac{dp}{dz}\right)_{Go} x^3 \quad (18)$$

where $\left(\frac{dp}{dz}\right)_{Lo}$ and $\left(\frac{dp}{dz}\right)_{Go}$ are the single phase frictional loss, respectively, for liquid and vapor states. They can be calculated by

$$\left(\frac{dp}{dz}\right)_{Lo} = f_L \frac{2\dot{m}_{total}^2}{D_{in}\rho_l} \quad (19)$$

and

$$\left(\frac{dp}{dz}\right)_{Go} = f_G \frac{2\dot{m}_{total}^2}{D_{in}\rho_g} \quad (20)$$

In the above equations, the friction factor and the Reynolds number are obtained from

$$f = \frac{0.079}{Re^{0.25}} \quad (21)$$

$$Re = \frac{\dot{m}_{total} D_{in}}{\mu} \quad (22)$$

using, respectively, the liquid and vapor properties.

3.5. Heat transfer coefficient inside the copper coil

A commonly used correlation of heat transfer coefficient for single phase flow is the Dittus–Boelter equation [21], in that

$$\alpha = 0.023\frac{Re^{0.8}Pr^{a}\lambda}{D_{\text{in}}} \tag{23}$$

where the exponent a is equal to 0.3 for liquid and 0.4 for vapor flow.

The local heat transfer coefficient for two-phase flow is calculated from a correlation which is based on the Lockhart–Martinelli parameter [16], in that

$$\alpha_{\text{r}} = \begin{cases} \alpha_{\text{tp}}(x) & (0 < x \leqslant x_{\text{d}}) \\ \alpha_{\text{tp}}(x_{\text{d}}) - [(x-x_{\text{d}})/(1-x_{\text{d}})]^2(\alpha_{\text{tp}}(x_{\text{d}}) - \alpha_{\text{v}}) & (x_{\text{d}} < x < 1) \end{cases} \tag{24}$$

$$\alpha_{\text{tp}}(x) = 3.4X_{\text{tt}}^{-0.45}\alpha_{l} \tag{25}$$

where α_{l} and α_{v} are the heat transfer coefficients for liquid and vapor calculated from Eq. (23) using the liquid and vapor properties, respectively; $x_d$is the dry-out vapor quality; X_{tt} is the Lockhart–Martinelli parameter which is expressed as:

$$X_{\text{tt}} = \left(\frac{\mu_{\text{l}}}{\mu_{\text{v}}}\right)^{0.1}\left(\frac{\rho_{\text{v}}}{\rho_{\text{l}}}\right)^{0.5}\left(\frac{1-x}{x}\right)^{0.9} \tag{26}$$

4. Discretization of the equations

To obtain a solution for the problem, the thermal collector plate is to be divided into small segments, as shown in Fig. 4. Two types of divisions are used. The first is along the refrigerant flow direction and the second is based on the *Y–Z* co-ordinate. With these two types of division, the temperature of a collector plate segment have two different forms of expressions: $T_{c,i}^{n+1}$ and $T_{c,j,k}^{n+1}$. To facilitate the programming procedure, transformation between the two different expressions is necessary. The matrix $\prod(j,k) = i$ according to the coil circuitry of the evaporator can be used to realize the transformation.

With the implicit finite difference method, the dynamic model of the PV evaporator can then be discretized as follows:

$$l_{\text{pv}}\rho_{\text{pv}}C_{\text{pv}}\frac{T_{\text{pv},j,k}^{n+1} - T_{\text{pv},j,k}^{n}}{\Delta t} = G(\tau\beta)_{\text{pv}} - E + \alpha_{\text{a-pv}}\left(T_{\text{a}} - T_{\text{pv},j,k}^{n+1}\right) + \alpha_{\text{r, a-pv}}\left(T_{\text{sky}} - T_{\text{pv},j,k}^{n+1}\right) + \frac{T_{c,j,k}^{n+1} - T_{\text{pv},j,k}^{n+1}}{R_{\text{pv-c}}} \tag{27}$$

$$\begin{aligned} m_{\text{c}}C_{\text{c}}\frac{T_{\text{c},j,k}^{n+1} - T_{\text{c},j,k}^{n}}{\Delta t} = {} & G(\tau\beta)_{\text{c}}(1-\xi)A_{\text{c}} + \alpha_{\text{a-c}}(1-\xi)A_{\text{c}}\left(T_{\text{a}} - T_{\text{c},j,k}^{n+1}\right) + \alpha_{\text{r, a-c}}(1-\xi)A_{\text{c}}\left(T_{\text{sky}} - T_{\text{c},j,k}^{n+1}\right) + \xi A_{\text{c}}\frac{T_{\text{pv}} - T_{\text{c},j,k}^{n+1}}{R_{\text{pv-c}}} \\ & + \alpha_{\text{r}}A_{\text{r}}\left(T_{\text{r},i}^{n+1} - T_{\text{c},j,k}^{n+1}\right) + \frac{A_{\text{c}}\left(T_{\text{a}} - T_{\text{c},j,k}^{n+1}\right)}{R_{\text{b}}} \\ & + \lambda_{\text{c,y}}l_{\text{c, y}}A_{\text{c}}\frac{T_{\text{c},j,k+1}^{n+1} + T_{\text{c},j,k-1}^{n+1} - 2T_{\text{c},j,k}^{n+1}}{\Delta y^2} \\ & + \lambda_{\text{c, z}}l_{\text{c, z}}A_{\text{c}}\frac{T_{\text{c},j+1,k}^{n+1} + T_{\text{c},j-1,k}^{n+1} - 2T_{\text{c},j,k}^{n+1}}{\Delta z^2} \end{aligned} \tag{28}$$

$$\frac{\rho_i^{n+1} - \rho_i^{n}}{\Delta t} + \frac{(\rho u)_i^{n+1} - (\rho u)_{i-1}^{n+1}}{\Delta z} = 0 \tag{29}$$

$$\rho_i^{n+1}\frac{u_i^{n+1} - u_i^{n}}{\Delta t} + (\rho u)_i^{n+1}\frac{u_i^{n+1} - u_{i-1}^{n+1}}{\Delta z} = -\frac{P_i^{n+1} - P_{i-1}^{n+1}}{\Delta z} - \left(\frac{\partial p}{\partial z}\right)_{\text{f},i}^{n+1} \tag{30}$$

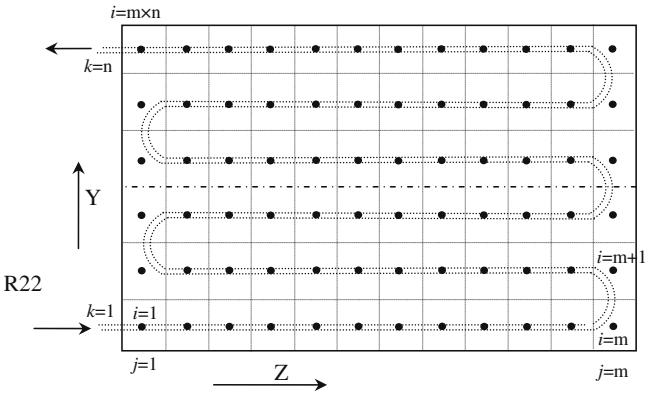

Fig. 4. Discretization scheme of the collector plate.

$$\frac{h_i^{n+1} - h_i^{n}}{\Delta t} + u_i^{n+1}\frac{h_i^{n+1} - h_{i-1}^{n+1}}{\Delta z} = \frac{\pi D_{\text{in}}}{\rho_i^{n+1}A}\dot{q}_{r,i}^{n+1} \tag{31}$$

In Eqs. (27)–(31), the integer n is for time step and i, j, k are for position identification.

5. Numerical simulation

To solve the above equation sets, initial distribution data of temperature, pressure and vapor quality for refrigerant as well as temperature for PV cells and thermal collector are required. The instantaneous boundary conditions, including solar irradiance, ambient temperature and inlet physical properties and mass flow rate of the refrigerant are also necessary. In order to investigate the dynamic behavior of the PV evaporator, a numerical simulation program written in C++ language has been developed.

Fig. 5 gives the flow chart of the computation process of the dynamic model. The program starts with assigning necessary initial values to the variables and setting the simulation time step to zero. Then the subroutines for computing the temperatures of the PV cell and the collector plate are called. The pressure, temperature, enthalpy, vapor quality and velocity of the refrigerant are then calculated based on the subroutines for Eqs. (29)–(31) and the auxiliary subroutines of the heat transfer coefficients, frictional pressure drop and refrigerant physical properties. The above processes are repeated until the relative error becomes small enough through iteration. Then the same calculations are repeated for all nodes with the advancement of the simulation time clock and up to the end of the simulation period.

6. Experimental setup

A schematic diagram of the PV/T-SAHP testing rig is shown in Fig. 6. An air-source evaporator and an air-cooled condenser are, respectively, connected in parallel with the PV evaporator and the water-cooled condenser. The PV cells of the evaporator are of single-crystalline silicon type having the following photovoltaic characteristics at standard testing conditions (i.e. at 1000 W/m^2 and 25 °C): 0.63 V open circuit voltage, 5.12 A short-circuit current, 2.40 W maximum power, 0.53 V and 4.58 A at maximum power point, and 15.4% electrical efficiency.

Four pressure sensors (Huba 506, accuracy ±0.5%) are located in the inlet and outlet of the evaporator and condenser to measure the pressure of the refrigerant. A mass flowmeter (Micromotion RS025, accuracy ±0.5%) is installed between the condenser and the expansion valve to record the mass flow of the refrigerant. Two wattmeters (accuracy ±0.5%) are used in the system to test the power consumption of the compressor and the output electric-

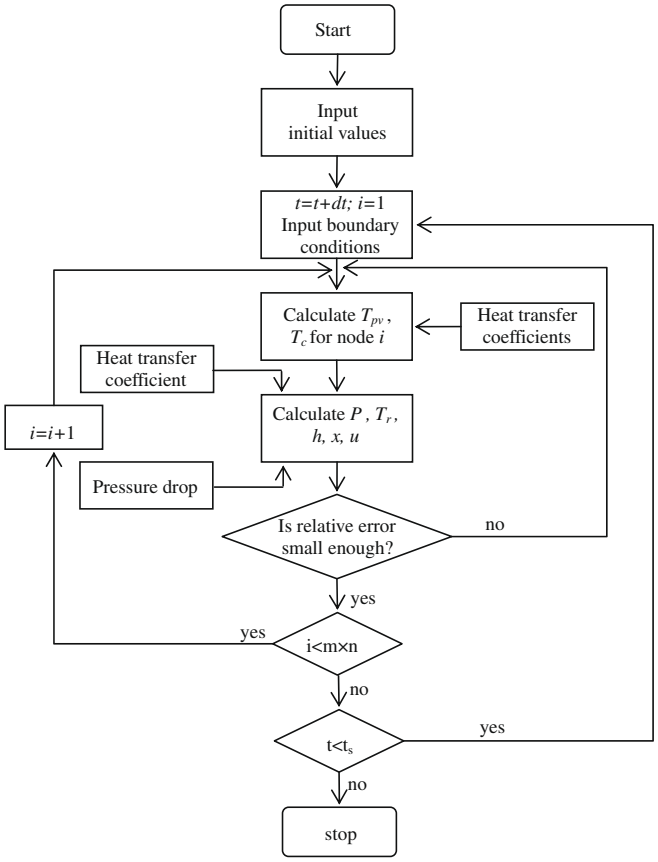

Fig. 5. Flow chart of the computer program of the PV evaporator.

ity of the PV evaporator, respectively. A solar pyranometer (TBQ-2, uncertainty about ±10 W/m^2) is mounted near the PV evaporator to measure the instantaneous solar radiation intensity. Numerous copper-constantan thermocouples (T-type, with uncertainty ±0.2 K) are used in the system to measure the temperature distribution of the system.

The experiment was carried out in Hefei, a city located at Central China at 31.87 °N and 117.23 °E. In our experimental tests, the PV evaporator and the water-cooled condenser were in service, with the supply temperature of the cooling water to the condenser kept constant and the compressor running at a constant frequency of 40 Hz.

7. Results and analysis

The solar irradiation and ambient temperature, which were monitored during the experiment period from 8:00 to 16:00, are shown in Fig. 7. It can be seen that the solar irradiation was from 200 to 840 W/m^2 and having the maximum value at noon. The ambient temperature increased from 279 K in the early morning to 287 K at about 13:30.

7.1. The pressure of the PV evaporator

The numerical and experimental data of the inlet and outlet pressures of the PV evaporator are compared in Fig. 8. It can be seen that the pressures generally increase with the solar irradiation. The predicted P_{in}, which is the fit values of the experimental inlet pressure of the evaporator, is adopted as the input boundary conditions of the simulation program. As can be seen in the figure, the experimental pressure drop was found much higher than the simulation prediction, and this resulted in an underestimation of the saturated temperature gradient. A corresponding higher temperature gradient along the copper coil was also observed during the experiment.

The simulation result of pressure distribution along the copper coil in the evaporator (with three modules in series) is given in Fig. 9. The frictional pressure drop was found increasing with the

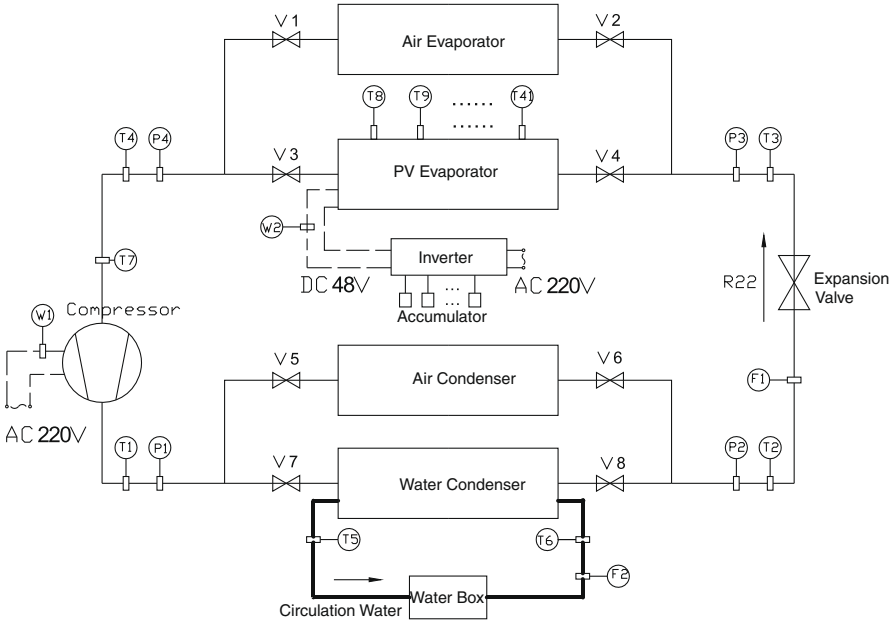

T1-T41, Thermocouples; V1-V8, Cut-off valves; P1-P4, Pressure sensors; F1-F2, Flow meters; W1-W2, Wattmeters

Fig. 6. Schematic diagram of the PV-SAHP experimental setup.

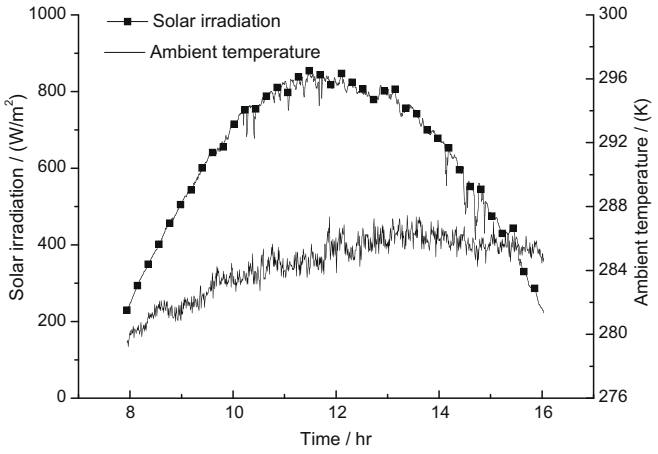

Fig. 7. The measured solar irradiation and ambient temperature.

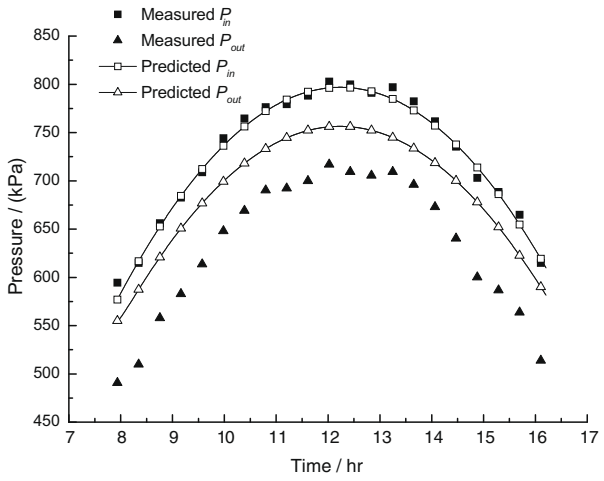

Fig. 8. Inlet and outlet pressures of the PV evaporator.

vapor quality in the two-phase flow region but declining in the dry-out region ($x > x_d$) [22]. In this graph, the slope of the pressure along the pipe escalates in the two-phase region but drops where the pipe length is at about 17 m.

7.2. The temperatures of the PV cells and solar collector

The thermocouples were located at the test point (Y = 0.835 m, Z = 0.9 m) of the middle module to monitor the temperatures of the PV cell and the thermal collector. The simulation and experimental results are given in Fig. 10. It can be seen that the simulation results show good agreement with the experimental data. The temperatures increase in the morning and reach their maximums at noon; the trend is therefore the same as the solar irradiation. A considerable temperature difference of 3–20 K between the PV cell and the collector plate can also be observed in this graph.

7.3. The electrical and thermal performance of the evaporator

Fig. 11 shows the output electricity and PV efficiency of the evaporator. The deviations of the predicted values from the experimental data were found within ±8%. The output electricity, ranging from 106 to 520 W, experiences the same trend as the solar irradiation. The PV efficiency however, shows a different trend with the output electricity. This is because the PV efficiency increases with τ_{eva} and declines with T_{pv} as illustrated in Eq. (8). In the early morning and late afternoon, τ_{eva} increases rapidly with the decline of the incidence angle of the solar beam. It remains almost constant from 10:00 to 14:00. Therefore, the PV efficiency approaches the "M" type curve with a tiny saddle at noon. It is also observed that both the simulation and experimental values of the PV efficiency are in good agreement and are above 12%. The performance is generally higher than those experienced in the water or air-type PV/T systems.

Fig. 12 shows the variation of the heat gain Q and thermal efficiency η_t of the evaporator. The heat gain generally increases with the solar irradiation. The thermal efficiency, which is above 50% during the testing period shows an opposite trend with the PV efficiency. The mean absolute deviation of the predicted and experimental values is about 10%. The absolute deviation in the early morning and late afternoon can reach 20% or higher. There exists an inflexion of the predicted values in the early morning due to the influence of the arbitrarily assigned initial values in the simulation program.

The numerical simulation of a direction expansion evaporator with the same boundary conditions has also been done. The average heat gain and the thermal efficiency are 2231 W and 68.1%, respectively, which are higher than the PV evaporator. Nevertheless, the PV evaporator can generate electricity and thermal energy

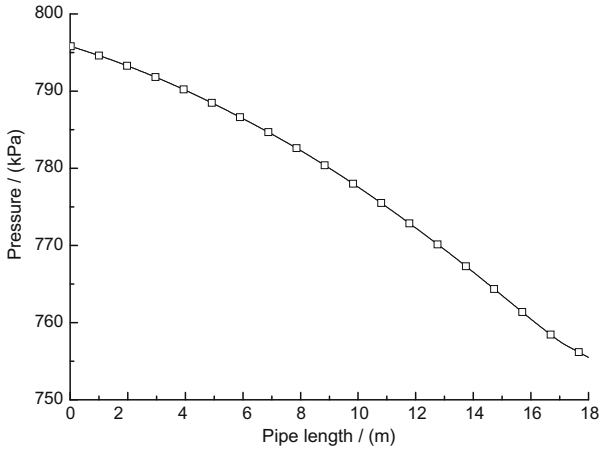

Fig. 9. Pressure distribution along the copper coil.

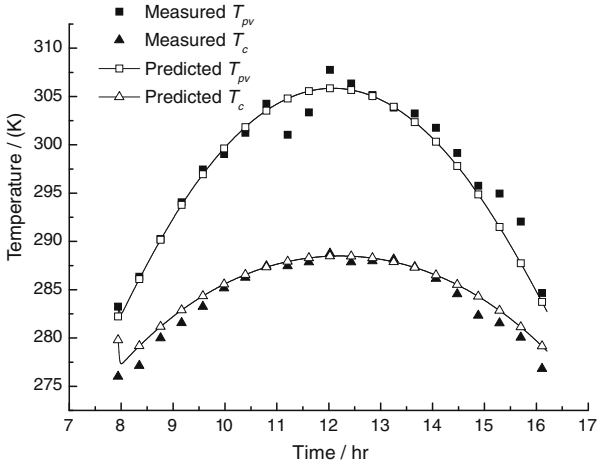

Fig. 10. Temperatures of the PV cell and thermal collector at test point.

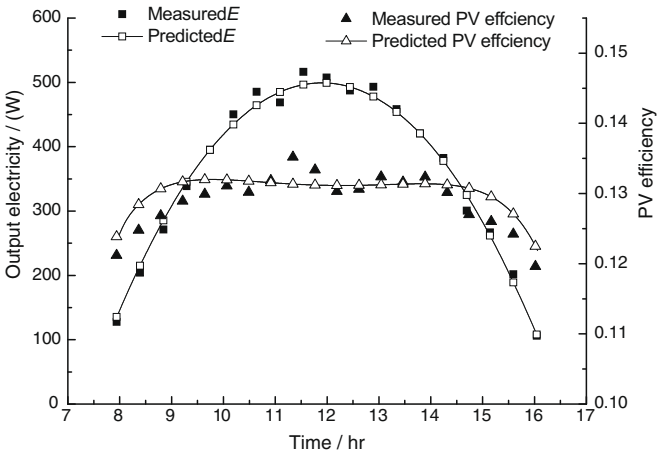

Fig. 11. The output electricity and PV efficiency of the evaporator.

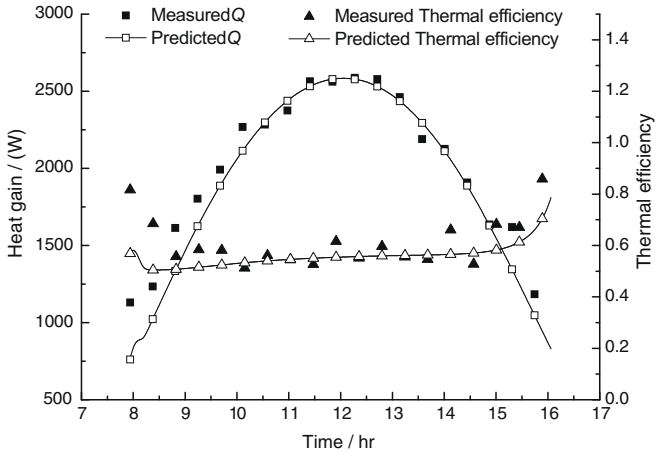

Fig. 12. The heat gain and thermal efficiency of the evaporator.

simultaneously. The evaluation presented by Huang [7] is introduced to describe the total performance of the PV evaporator.

$$Q_{\text{total}} = Q + \frac{E}{0.38} \tag{32}$$

$$\eta_{\text{total}} = \eta_{\text{t}} + \frac{\eta_{\text{pv}}}{0.38} \tag{33}$$

where Q_{total} and η_{total} are the total heat gain and total efficiency of the PV evaporator, respectively.

With Eq. (32,33), the average total heat gain and total efficiency of the PV evaporator are 2997.8 W and 95.6% which are much higher than the direct-expansion evaporator.

7.4. The temperature distribution of the evaporator along the coil

The predicted temperatures of the thermal collector, PV cells, and refrigerant along the coil at 12:00 are illustrated in Fig. 13. The temperature lines decline along the coil in the two-phase region due to the pressure drop, but increase rapidly in the superheated region. The temperature difference between the PV cells and the thermal collector is much higher than that between the thermal collector and the refrigerant.

Two-dimensional temperature distribution of the collector plate is depicted in Fig. 14. The temperature changes along the Z direction are much smaller than those along the Y direction. Because of the shadows cast by the frames, the effective collector area

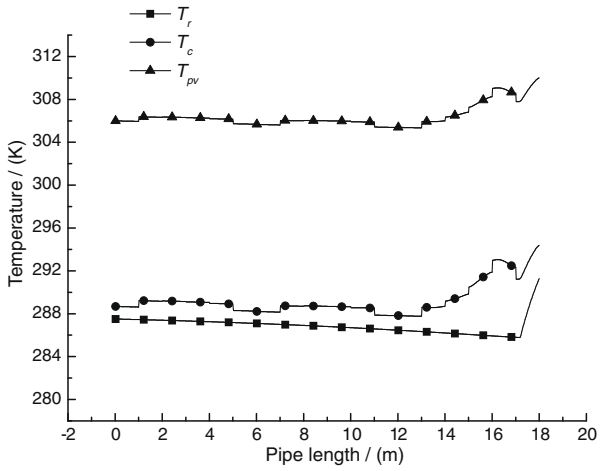

Fig. 13. The temperatures distribution along the copper coil of the evaporator.

for the peripheral nodes along the Z direction in every evaporator module is slightly smaller than that of the other nodes. Hence, the temperature line shows a zigzag trend in the two-phase flow region. The temperature drop along the flow direction in the superheated region is owing to the heat conduction of the nodes with the others in the two-phase flow region along the Y direction.

7.5. The distribution of the vapor quality and average specific enthalpy

The distribution of the vapor quality and average specific enthalpy of the refrigerant can also be predicted by our program. The simulation results at 12:00 are depicted in Fig. 15. It can be observed that the vapor quality varies almost linearly in the two-phase flow region and remains constant in the superheated region. A similar trend of the average specific enthalpy is also observed.

7.6. Error analysis

The experimental error of the independent variables, such as pressure, temperature, mass flow, output electricity and solar irradiation, is determined by the accuracy of the corresponding instrument. While the experimental error of the dependent variables, such as Q, η_t andη_{pv} can be calculated from the experimental error

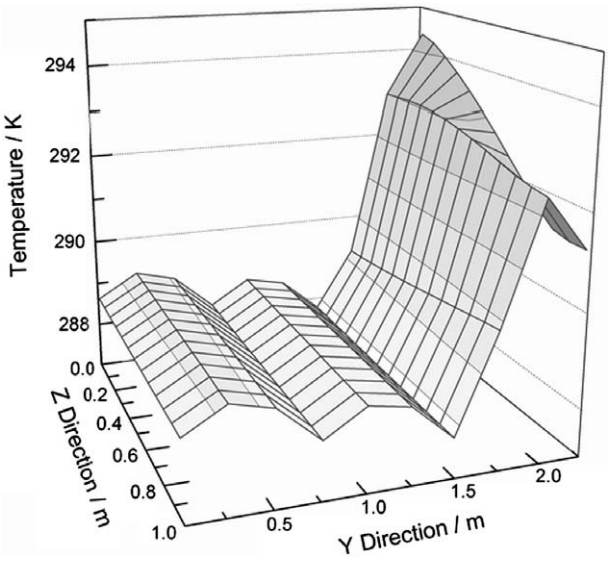

Fig. 14. Two-dimensional temperature distribution of the thermal collector.

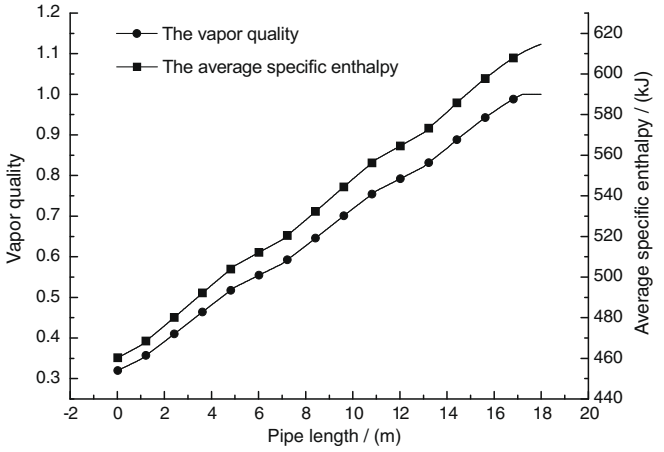

Fig. 15. Refrigerant vapor quality and specific enthalpy along the copper coil.

Table 1
The experimental RME of the variables

Variable	P_{in}	P_{out}	T_w	E	η_{pv}	Q
RME	0.5%	0.5%	0.064%	0.5%	1.79%	22.9%

of the independent variables according to the theory of error propagation. Given a dependent variable y, its function can be expressed as follows:

$$y = f(x_1, x_2, \ldots, x_n) \tag{34}$$

where x_i, ($i = 1, \ldots, n$) is the variable of the function.

The relative error (RE) of dependent variable y can be expressed as follows:

$$\mathrm{RE} = \frac{\mathrm{d}y}{y} = \frac{\partial f}{\partial x_1}\frac{\mathrm{d}x_1}{y} + \frac{\partial f}{\partial x_2}\frac{\mathrm{d}x_2}{y} + \cdots + \frac{\partial f}{\partial x_n}\frac{\mathrm{d}x_n}{y} \tag{35}$$

where $\partial f/\partial x_i$ is the error transferring coefficient of the variables.

The experimental relative mean error (RME) during the testing period can be defined as:

$$\mathrm{RME} = \frac{\sum_1^N |\mathrm{RE}|}{N} \tag{36}$$

Therefore the experimental relative mean error (RME) of the dependent variables can be obtained according to their function and Eq. (34). The MRE of all variables discussed is listed in Table 1.

8. Conclusions

A novel photovoltaic/thermal solar-assisted heat pump (PV/T-SAHP) system, which can generate electricity and heat energy simultaneously, is presented in this paper. A mathematical model based on the distributed parameter technique has been introduced for predicting the dynamic system behavior. Corresponding experiment has been carried out to test the actual performance and to verify the numerical model. The PV efficiency was found above 12%, which is higher than the performance in the other types of PV/T system. Better cooling effect of the PV cells is therefore confirmed in this system. Simulation results, such as temperature, output electricity and heat gain show satisfactory agreement with the experimental data. The deviations of the predicted and measured output electricity and PV efficiency are within ±8%. The mean absolute deviations of the heat gain and thermal efficiency are about 10%. Notwithstanding these, the model underestimates the refrigerant pressure drop at the PV evaporator.

Acknowledgements

The work in this paper was sponsored by the National Natural Science Foundation of People's Republic of China (Project Nos. 50478023 and 50708105) and Anhui Province Science Foundation of China (Project No. 070414161).

References

[1] P. Sporn, E.R. Ambrose, The heat pump and solar energy, Proceedings of the World Symposium on Applied Solar Energy, Phoenix, Arizona, 1955.
[2] S.K. Chaturvedi, D.T. Chen, A. Kheireddine, Thermal performance of a variable capacity direct expansion solar assisted heat pump, Energy Convers. Manage. 39 (1998) 181–191.
[3] E. Torres Reyes et al., Energy analysis and optimization of a solar-assisted heat pump, Energy 23 (1998) 337–344.
[4] J.G. Cervantes, E. Torres-Reyes, Experiments on a solar-assisted heat pump and an energy analysis of the system, Appl. Ther. Eng. 22 (2002) 1289–1997.
[5] Y.H. Kuang, R.Z. Wang, Performance of a multi-functional direct-expansion solar assisted heat pump system, Solar Energy 80 (2006) 795–803.
[6] B.J. Huang, J.P. Chyng, Performance characteristics of integral type solar assisted heat pump, Solar Energy 71 (2001) 403–414.
[7] J.P. Chyng, C.P. Lee, B.J. Huang, Performance analysis of a solar-assisted heat pump water heater, Solar Energy 74 (2003) 33–44.
[8] E.C. Kern Jr., M.C. Russell, Combined photo-voltaic and thermal hybrid collector systems, Proceedings of the IEEE Photovoltaic Specialists, Washington, DC, USA, 1078, pp. 1153–1157.
[9] B.J. Huang, T.H. Lin, W.C. Hung, F.S. Sun, Performance evaluation of solar photovoltaic/thermal systems, Solar Energy 70 (2001) 443–448.
[10] T.T. Chow, W. He, J. Ji, Hybrid photovoltaic–thermosyphon water heating system for residential application, Solar Energy 80 (2006) 298–306.
[11] T.T. Chow, W. He, J. Ji, A.L.S. Chan, Performance evaluation of photovoltaic–thermosyphon system for subtropical climate application, Solar Energy 81 (2007) 123–130.
[12] Jie Ji, Jian-Ping Lu, Tin-Tai Chow, Wei He, Gang Pei, A sensitivity study of a hybrid photovoltaic/thermal water-heating system with natural circulation, Applied Energy 84 (2007) 222–237.
[13] J.K. Tonui, Y. Tripanagnostopoulos, Air-cooled PV/T solar collectors with low cost performance improvements, Solar Energy 81 (2007) 498–511.
[14] J. Prakash, Transient analysis of a photovoltaic/thermal solar collector for co-generation of electricity and hot air/water, Energy Convers. Manag. 35 (1994) 967–972.
[15] J.W. MacArthur, E.W. Grald, Unsteady compressible two-phase flow model for predicting cyclic heat pump performance and a comparison with experimental data, Int. J. Refrig. 12 (1989) 29–41.
[16] H. Wang, S. Touber, Distributed and non-steady-state modeling of an air cooler, Int. J. Refrig. 14 (1991) 98–111.
[17] X. Jia, C.P. Tso, P. Jolly, Y.W. Wong, Distributed steady and dynamic modeling of dry-expansion evaporators, Int. J. Refrig. 22 (1999) 126–136.
[18] T.T. Chow, Performance analysis of photovoltaic-thermal collector by explicit dynamic model, Solar Energy 75 (2003) 143–152.
[19] J.A. Duffie, W.A. Beckman, Solar Engineering of Thermal Processes, second ed., Wiley, New York, 1991.
[20] H. Müller-Steinhagen, K. Heck, A simple friction pressure drop correlation for two-phase flow in pipes, Chem. Eng. Process. 20 (1986) 297–308.
[21] F.W. Dittus, L.M.K. Boelter, University of California (Berkeley), Pub. Eng., vol. 2, 1930, p. 443.
[22] M.B. Ould Didi, N. Kattan, J.R. Thome, Prediction of two-phase pressure gradients of refrigerants in horizontal tubes, Int. J. Refrig. 25 (2002) 935–947.